Binary oxide composite adsorbent for copper, nickel and zinc cations removal from aqueous solutions

O.A. Abdel Moamen*, H.S. Hassan, E.A. El-Sherif

*Hot Lab. Center, Atomic Energy Authority of Egypt, Cairo, Egypt, Tel. +20 1001336124, Fax +20 244620772,
email: eng-olaa@hotmail.com (O.A.A. Moamen), hisoliman2000@yahoo.com (H.S. Hassan), Dr_Eman1961@hotmail.com (E.A. El-Sherif)*

ABSTRACT

The synthesized ultra-microporous zirconium–magnesium bimetal oxide was adroitly synthesized via the use of sol-gel technique. The synthesized composite was applied in the adsorption of copper, nickel and zinc cations from aqueous solutions. The composite properties were characterized by X-ray diffraction (XRD), Surface area (BET) by nitrogen adsorption–desorption, Thermo-gravimetric measurement (TG/DTG) and Fourier transformed infra-red (FTIR). The surface morphology of the synthesized composite was studied via the use of scanning electron microscopy (SEM) and fractal dimension concept. The influence of initial pH on sorption of copper, nickel and zinc cations in terms of removal efficiency was studied and deduced that the removal increases significantly with increasing the pH from 3 to 11. The intra-particle kinetic diffusion model confirmed that the adsorption mechanism controlled by multi-diffusion steps, comprising both film and intra-particle diffusion. The Toth isotherm model was elected to represent equilibrium of the concerned cations adsorption onto the composite. The thermodynamic parameters were calculated via the use of Flory-Huggins model.

Keywords: Ultra-microporous zirconia–magnesia composite; Fractal dimension analysis; Zn^{2+}; Cu^{2+} and Ni^{2+} adsorption; Process parameters optimization; Adsorption mechanism study

1. Introduction

Heavy metals pollution is a serious threat to aquatic ecosystems, as some of these metals are potentially venomous, even at extremely low concentrations. Moreover, heavy metals are non biodegradable and have a tendency to accumulate in living organisms, and causing harsh problems to both human health and wildlife [1]. Several industries contain heavy metals in its discharged waters for instant metal coating, battery production, and mining. Copper, Zinc and nickel are amongst the most popular heavy metals in these wastewaters. The accumulation of copper in human body causes skin, pancreas, brain and heart diseases. Zinc is the main element for life and acts as micronutrient when exist in trace quantities. The world health organization recommended the maximum permissible concentration of zinc in water as 5.0 mg/L. Beyond this limit, zinc is toxic and cause incoordination in muscles, dizziness, stomachache and nausea [2].

Nickel can be found in nature in two oxidation states, namely zero (Ni^{0+}) and divalent nickel (Ni^{2+}). Ni^{2+} is poisonous to most organisms for concentrations > 0.05 mg/L. Higher nickel concentrations cause lungs cancer, sickness, dizziness, vomiting, chest pain, dry cough ,tightness of the chest, shortness of breath, cyanosis, rapid respiration and extreme weakness [3].

Different techniques for instant membrane technology, electrolytic reduction, chemical precipitation/coagulation, ion exchange and adsorption are used for the treatment of wastewater containing these cations. The main advantages and disadvantages related to each method are reviewed elsewhere [4]. Adsorption is one of the most widespread methods used for removal of heavy metal ions owing to its convenience, simplicity and high removal efficiency [5]. Organic and inorganic adsorbents are two accessible adsor-

*Corresponding author.

bents but inorganic adsorbents have been demonstrated to be a widespread water treatment material, including various metal oxides [6,7].

In comparison with the activated porous carbon, metal oxides are more promising perspectives owing to the following aspects: (i) metal oxides have a good selectivity towards heavy metals; (ii) metal oxides can be easily synthesized into granule particles with different sized or be in situ formed to realize engineering application [8]. Zirconium oxide has a strong affinity to heavy metals and high resistance to attack via alkalis, acids, reductants and oxidants [7]. Magnesium oxide has a very important role in contaminated aqueous solutions treatment as it has the ability to remove effectively various heavy metals. It has been of great concern to industrial and academia communities to incorporate some metal oxides into zirconia to prepare bimetal oxides which may show more brilliant physicochemical properties and higher sorption capacity than their single metal oxide [9,10]. Thus, a zirconium-magnesium bimetal oxide composite originating from the combination of magnesium oxide and zirconium oxide is predictable to show a great potential for copper, nickel and zinc cations removal.

Apart from the well-documented effect factors such as pH, ionic strength, time, initial contaminant concentration, previous studies also revealed that the pore structure and particle size of sorbents played an important role in sorption performance. Ultra-microporous materials with suitable size distribution and desired pore structure are aspired to produce a high adsorptive sites density. Bi-metal oxides with ultra-microporous structures have large pore volume; adjustable pore diameters and specific surface area [11,12], which are desirable characteristics for adsorption. Some microporous materials, including carbon, silica and metal oxides [12,13], have been tested for removal of several heavy metals, but the results were not satisfactory. Either the adsorption capacity was lower than 23 mg/g or adsorbent synthesis procedure required high temperature of about 673–873 K which as a result increased the synthesis cost. Consequently, it is in strong demand to develop a new synthesis route for the preparation of ultra-microporous material with high Zn^{2+}; Cu^{2+} and Ni^{2+} removal efficiency. In this work, a sol-gel technique was established to synthesize an innovative ultra-microporous zirconium-magnesium bimetal oxide. The major aims of this work are to (i) characterize the novel synthesized zirconia-magnesia composite; (ii) Study the roughness and surface irregularities of the synthesized composite via fractal dimension analysis (iii) compare and assess Zn^{2+}; Cu^{2+} and Ni^{2+} adsorption performance and lastly; (iii) demonstrate the adsorption mechanism via the use of numerous kinetic and thermodynamic models.

2. Experimental

2.1. Materials and synthesis procedure of zirconia-magnesia composite

Reagents used in this work were of analytical grade and purchased from Merck Company. The stock solution of 100 mg/l copper chloride ($CuCl_2$); nickel chloride ($NiCl_2$) and zinc chloride ($ZnCl_2$) were prepared by dissolving 1 g salt ion in 1 L bidistilled water. Other $CuCl_2$; $NiCl_2$ and $ZnCl_2$ solutions were obtained by diluting the 100 mg/l stock solution with deionized water. Bidistilled water was used to cleanse the synthesized zirconia-magnesia composite and prepare contaminants solutions. Both HCl and NaOH solutions were utilized as pH regulator. The preparation of Ultra-microporous ZrO_2-MgO composite particles involves the resin formation between urea and formaldehyde using $MgCl_2$ and $ZrCl_4$ as a precursor. Urea-formaldehyde resin was synthesized via the condensation reaction amid urea and formaldehyde in alkaline condition at a temperature ranged between 60–70°C throughout resin formation for about 1 h. The reaction started at pH value of about 8.5 during stirring and terminated at pH value of 1.5 through simultaneous addition of ethylene glycol and ZrO_2; MgO salt solutions. The formed gel was prepared using urea, formaldehyde, ethylene glycol, zirconium chloride and magnesium chloride in a ratio of 1:1:1:2:2. Transparent polymeric gel had been attained with no signs of precipitation, in which salt cations are occluded in the structure. The reaction products were eliminated under reduced pressure using a pump. The produced gel was slowly dried via two steps: a first drying at 80°C followed by a second at 120°C to avoid damage as a result of drying stresses (spalling) and thermal shock. The flow chart of preparation procedure is displayed in Fig. 1.

2.2. Sorbent Characterization

The X-ray diffraction (XRD) pattern of the synthesized sorbents was determined by Schimadzu X-ray diffractometer (Cu Kα radiation = 1.5406 A) over a range of 20°–60° operated at 30 mA and 40 kV, with a scan rate of 8°/min and sampling pitch of 0.02°. Fourier transformed infrared spectrometry test (FTIR) was utilized for the verification of the composite structure. The IR spectra were collected via PerkinElmer, BX spectrometer among a frequency range of 4000–450 cm^{-1}. Thermo- gravimetric measurement (TG/DTG) was performed with a DTG-60/DTG-60A-Shimadzu-Japan from 338 to 1288 K at a heating rate of 35 K min^{-1} in N_2 atmosphere. Specific surface area of the composite was determined using standard volumetric method via nitrogen adsorption at 77 K and application of BET equation through Nova 3200 BET instrument, Quantachrome Corporation, USA.

Scanning electron microscopy (SEM) was carried out with a (SEM, JEOL, JEM 1000CX). There are various ways for computing the pore distribution fractal dimension (D1) of a SEM image, for instance box-counting method, Fourier method and probability statistics method. The box-counting method was applied via the use of Fraclac. Program and D_1 is calculated via Eq. (1) [14] as:

$$D_1 = -\lim_{\delta \to 0} \frac{\ln(N(\delta))}{\ln(\delta)} \tag{1}$$

where $N(\delta)$ is the boxes number required to totally cover the binary image and δ is the boxes length. Eq. (1) can be rewritten as follows [15]:

$$\ln(N(\delta)) = -D_1 \ln(\delta) + cons\tan t \tag{2}$$
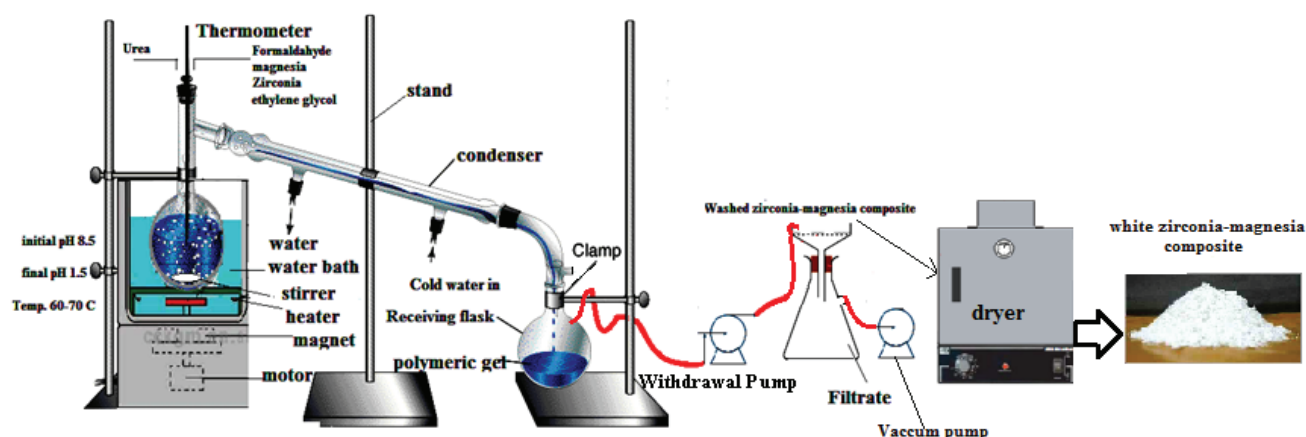
Fig. 1. Synthesis procedure of Zirconia-Magnesia powder.

Consequently, the box-counting dimension (fractal dimension) can be verified from the slope of a linear plot of $\ln(N(\delta))$ Vs. $\ln(\delta)$. The fractal dimension approximated for this simple image is about 1.62. Before determining the fractal dimension, the thresholding process must be carried out. Thresholding process refers to the transformation of a colored image into black and white. The box size (r) is changing from 1 pix to 400 pix. For each mesh size the black and black and white boxes number is counted and the fractal dimension is estimated.

2.3. Batch adsorption studies

The sorption behavior of Zn^{2+}; Cu^{2+} and Ni^{2+} onto the synthesized composite as a function of pH, initial cation concentration, ionic strength and temperature was investigated by batch technique. The sorption equilibrium data were analyzed using non-linear Langmuir, Freundlich, Temkin, Toth and Flory–Huggins isotherm models to evaluate the sorption characteristics. The kinetics of adsorption reaction is also assessed using known models and the relevant parameters were evaluated. All sorption experiments were performed in a well-capped 50 mL shaker tubes. 100 ml cations solution with required concentration and 0.1 g composite were added into a tube and then the tube was shaken in a thermostatic shaker with 1000 rpm at 298 K for 24 h. After shaking, the adsorbent was separated by a well-capped centrifuge tubes. The residual cation concentration in the filtrate was determined spectrophotometrically using atomic absorption spectrophotometer (Buck Scientific, VGP 210). The value of solution's pH was adjusted via the use of dilute HCl and NaOH solutions. The initial Zn^{2+}; Cu^{2+} and Ni^{2+} concentration, initial pH and solution volume to adsorbent dosage ratio (V/m) were fixed at 50 mg/l, 7 ± 0.01, and 100 ml/g, respectively, unless otherwise stated. Sorption isotherms were studied by varying initial Zn^{2+}; Cu^{2+} and Ni^{2+} concentration from 50 to 700 mg/l.

2.3.1. data analysis

Dynamic and equilibrium investigations were performed at pH 7± 0.01 using the same V/m ratio and at three different temperatures (298, 318 and 333 K). The equilibrium amounts of the concerned cations adsorbed onto the synthesized material, q_e (mg/g) were estimated using;

$$q_e = \int_{i=1}^{n} \frac{(C_0 - C_t) \cdot V}{m} \qquad (3)$$

where i, n, q_e, C_o, m and V is the experimental data points number, maximum experimental data points, equilibrium capacity (mg/g), initial cation concentration (mg/L), adsorbent mass (g) and solute ions volume (L) respectively. The Equilibrium sorption isotherm studies were performed by stirring the synthesized composite overnight with different solutions of changeable initial cation concentration in the range of 50–700 mg/L.

A. Adsorption isotherm models

Generally, the adsorption isotherm is a very helpful curve depicting the phenomenon governing the retention or mobility of a substance from aquatic environment to a solid-adsorbent at a constant temperature and pH. A variety of equilibrium isotherm models (Langmuir, Freundlich, Temkin, Toth and Flory–Huggins isotherm), have been used in regard of three fundamental approaches [16–18].

Langmuir adsorption isotherm model supposes that the thickness of adsorbed layer is one molecule (monolayer adsorption) and the adsorption can only take place at a finite number of definite localized sites which are identical and equivalent, with no profiling interaction and steric hindrance amid the adsorbed molecules [19,20]. It also presumes that the adsorption is homogeneous and each molecule has constant enthalpies and sorption activation energy [21]. The non-linear langmiur model can express as:

$$q_e = \frac{Q^0 b C_e}{1 + b C_e} \qquad (4)$$

where, q_e is the composite sorption capacity (mg/g) at equilibrium solute concentration, C_e (mg/L), in the aqueous phase, Q° and b are the Langmuir constants concerned with the adsorption capacity and energy, respectively.

The multilayer formation can be examined by the Freundlich isotherm model [22]) which supposes that the

sorbent has a heterogeneous valance distribution having different affinity for adsorption. This model takes the subsequent form:

$$q_e = K_f C_e^{1/n} \tag{5}$$

where K_f and n are the Freundlich adsorption capacity and sorbent intensity, respectively. The maximum adsorption capacity is determined by the constant initial cation concentration C_o and changeable adsorbent weights as:

$$K_f = \frac{q_m}{C_o^{1/n}} \tag{6}$$

where q_m is the Freundlich maximum adsorption capacity (mg/g) and C_o is the initial solute concentration in the bulk solution (mg/l).

Both Langmuir and Freundlich models have special prominence to demonstrate the ideal case of chemisorption or physisorption on surface enclosing finite number of identical sites. A number of non-ideal effects can be clarified by numerous mathematical expressions like Temkin; Toth and Flory-Huggins models.

Temkin isotherm model usually used for heterogeneous surface energy systems (non-uniform distribution of sorption heat) and represented as [23]:

$$q_e = \frac{RT}{b_t} \ln(a_t C_e) \tag{7}$$

where b_t is the Temkin constant that represent the adsorption heat (KJ/mol), R is gas constant, a_t is the isotherm constant and T is absolute temperature in Kelvin.

Toth isotherm model [24], is an empirical equation regarded to give a broad range of fit than both Freundlich or Langmuir model and is useful in depicting adsorption systems, at high and low adsorbate concentrations. The non-linear Toth equation is represented as (Eq. (8)):

$$q_e = \frac{q_T K_T C_e}{\left[1 + (K_T C_e)^n T\right]^{\frac{1}{n_T}}} \tag{8}$$

where q_T, K_T and n_T are the Toth isotherm parameters. Once n_T is equal to 1, it proposes that the adsorption takes place on a homogeneous surface. While, for heterogeneous adsorbents, n_T is lower than 1.

Flory–Huggins isotherm model [25] can be used to obtain the surface coverage characteristics degree of adsorbate onto the adsorbent and can elucidate the feasibility and spontaneous nature of the adsorption process. The Flory–Huggins isotherm model can be expressed as:

$$\frac{\theta}{C_0} = K_{fh}(1-\theta)^{\eta_{fh}} \tag{9}$$

where θ represents the surface coverage degree $\theta = 1 - C_e / C_0$ and K_{fh} ; η_{fh} stands for the augury of model equilibrium constant and exponent. The temperature influence on the dynamics of the cations adsorption process was studied using Clausius-Clapeyron's thermodynamic equation [26]. The differential form of Clausius-Clapeyron equation is illustrated as:

$$\frac{d\ln K_{fh}}{dT} = \frac{\Delta H^0}{RT^2} \tag{10}$$

After integrating the above differential equation becomes:

$$\ln K_{fh} = \frac{\Delta H^0}{RT} + C \tag{11}$$

Legitimately applying $\Delta G^0 = -RT\ln(K_{fh})$ and $\Delta G^0 = \Delta H^0 - T\Delta S^0$

$$then, \ln(K_{fh}) = \frac{\Delta S^0}{R} - \frac{\Delta H^0}{RT}$$

where R is the gas constant, 8.314 J/mol·k; ΔH^0 is the Enthalpy (kJ/mol) ; ΔS^0 is the Entropy (J/mol/K) and T is absolute temperature in Kelvin.

B. Adsorption dynamics

B.1. The adsorption reaction

The major issue when searching for a suitable adsorption mechanism is to elect a mathematical model that is not only fits the experimental data with acceptable accuracy but also complies with a reasonable adsorption mechanism. Fractal like-pseudo-first and -second order kinetic models were utilized to fit the experimental data. The fractal like-pseudo-first order kinetic model (FL-PFO) presumes the adsorption of one adsorbate molecule onto one active site on the adsorbent surface. The modified fractal-like first order model can be represented as [26]:

$$q_t = q_e(1 - e^{-k_t \cdot t^\varphi}) \tag{12}$$

The modified fractal-like fractal like-pseudo-second order kinetic model (FL-PSO) assumes that one adsorbate molecule is adsorbed onto two active sites that can be written as [26]:

$$q_t = \frac{(K_2 q_e^2 \cdot t^\varphi)}{(1 + K_2 q_e \cdot t^\varphi)} \tag{13}$$

where q_e and q_t are the amounts of cations adsorbed at both equilibrium (mg/g) and fractal time $t\varphi$ (min); k_1 (min⁻¹) and k_2 (g·mg⁻¹·min⁻¹) are the fractal like fractal like-pseudo-first- and -second-order rate constants, respectively. Both the FL-PFO and FL-PSO models cannot be utilized to recognize the diffusion mechanism, thus the intra-particle diffusion model was intended.

B.2. Intra-particle diffusion model

In solid–liquid adsorption systems, mass transport can be depicted via a three main steps that is external mass transfer from the bulk solution to the solid surface; intra-particle diffusion and finally adsorption onto the adsorbent surface site. The intra-particle diffusion effect on the adsorption kinetics was investigated by Weber and Morris at which the mathematical reliance of q_t against $t^{1/2}$ is attained if the process is believed to be affected by diffusion in the particles and convective diffusion in the

solution [26] thus the root time reliance may be stated by the subsequent equation:

$$q_t = K_{int}.t^{0.5} + I \tag{14}$$

where q_t is the amount of cation on the adsorbent surface (mg/g) at fractal time t (min), k_i is the fractal like intra-particle diffusion rate constant (mg/g·min$^{0.5}$) and I is a constant that signifies the boundary layer thickness. The larger the I value, the thicker the boundary layer. If the plot of q_t against $t^{0.5}$ is a straight line then the intra-particle diffusion is the rate-limiting step, whilst if there is more than one straight line, the entire process can be split into particular steps of mass transfer.

2.3.2. Theory treatments

Nonlinear Chi-square (χ^2) test is a statistical tool for error analysis that is needed for the best fit of the data [Eq. (15)]. It is obtained by judging the sum squares difference amid the experimental and calculated data, with each squared difference is divided by its corresponding value [27]. The value of chi-square is calculated by using this equation:

$$x^2 = \sum_{i=1}^{n} \frac{(q_{e,model} - q_{e,Exp.})^2}{q_{e,Exp.}} \tag{15}$$

3. Results and discussion

3.1. Characterization of the synthesized adsorbent

The powder XRD pattern of the synthesized material is illustrated in Fig. 2a. It can be seen that the synthesized material consists mainly of ZrO_2-MgO. The appeared ZrO_2 includes two crystalline phases. The first phase is monoclinic, marked by the red circles. The detected second phase demonstrates presence of tetragonal lattice structure, marked with the blue squares [18]. By comparing the two crystalline zirconia phase intensities, it can be found that the monoclinic zirconia phase is the chief component in the
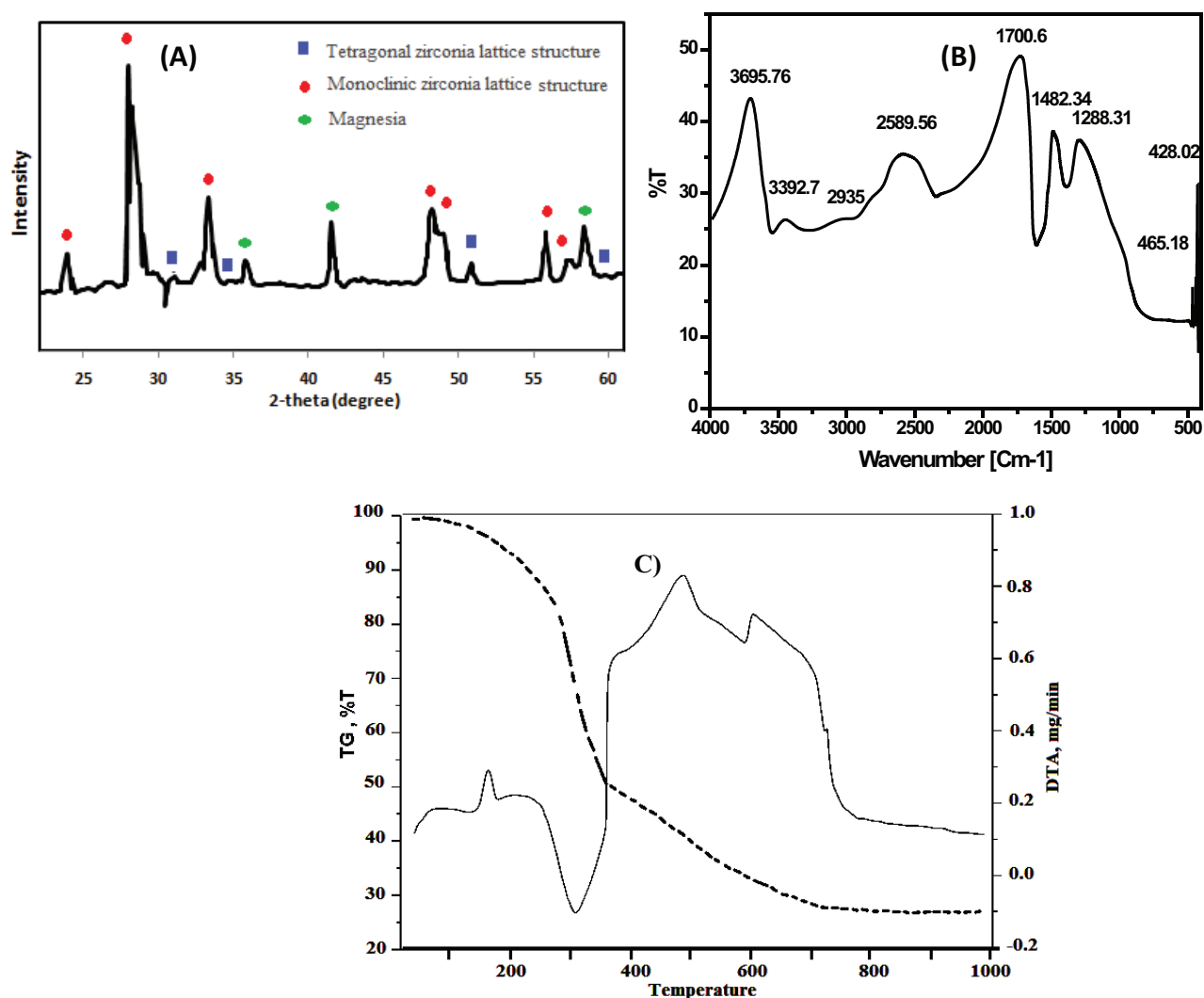
Fig. 2. Characterization tests of the synthesized composite.

solid mixture. The composite peaks at 36.92, 42.9 and 59.28 in agreement with the phase of MgO represented by green circles [28] The XRD pattern demonstrated that the synthesized material consists mainly of magnesia and zirconia exhibiting a crystalline structure.

The FT-IR spectrum of the composite (Fig. 2b) characterized by the presence of eight characteristic peaks at 428.02, 465.18, 1288.31, 1482.34, 1700.6, 2589.56, 3392.7 and 3695.76 cm^{-1} is illustrated in Fig. 2b. The absorption peaks in the stretching region of 3700–3000 cm^{-1} assigned to the vibration of –OH on the surface of ZrO_2–MgO composite, whereas the bending of the physically bonded water H–O–H is situated at about 1700 cm^{-1} [29]. The absorption peaks appeared at 465.18 cm^{-1} coincided with the stretching vibration of Zr–O. Another important absorption bands can be observed at 428 and 1288 cm^{-1} which is related to the vibration of the Mg-O bond. The appeared peaks at 1482 cm^{-1} are owing to the bending vibration of Zr–OH groups [30].

The DTA and TG curves for the synthesized composite are shown in Fig. 2C. The DTA curve showed that the prepared material has two dehydration steps at 310.40 and 594.40 that attributed to the variance in bonding strength of the water molecules attached to composite structure. The first endothermic region in composite range from 260 to 380°C with a peak at about 310.40°C corresponds to the formation of oxide bridge accompanied by loss of adsorbed water molecules [31]. The total weight loss is about 70% of the initial composite weight and the final loss takes place at 1000°C. The specific surface area, total pore volume and average pore diameter of the synthesized composite are 65.42 m^2/g, 0.06 cm^3/g, and 1.25 nm, respectively, calculated via the use of the standard BET method. Fig. 3 illustrates the original gray-scale SEM image; the binary colored image; free layout SEM image and SEM box coverage with boxes length of δ. The ln(N(δ)) vs. ln(δ) plots are illustrated in Fig. 3. The entire plots exhibit good fits with correlation coefficients > 0.99, which shows that the pore distributions on the composite surface are fractal. The D_1 value on composite surface is 1.6208 revealing that the pore distribution and composite surface are heterogeneous.

3.2. Optimization of process parameters

3.2.1. Effect of initial pH

The adsorption of the concerned cations onto the synthesized composite with varying pH is given in Fig. 4A.
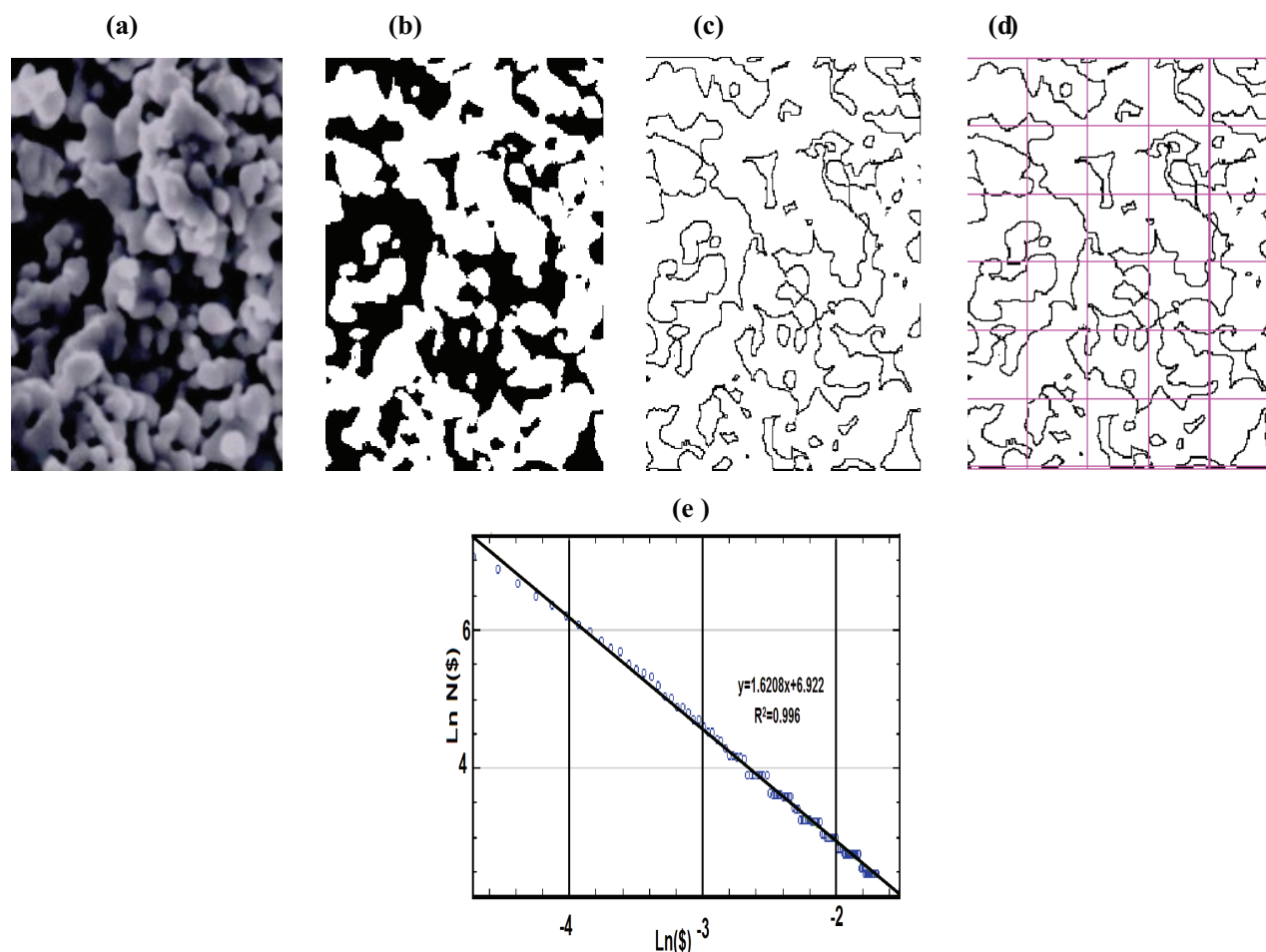
Fig. 3. The box-counting method procedure for fractal dimension D of the synthesized material: (a) The original gray-scale SEM image; (b) binary colored image; (c) Free layout SEM image; (d) box coverage; (e) D_1 calculation results from ln(N(δ)) vs. ln(δ).
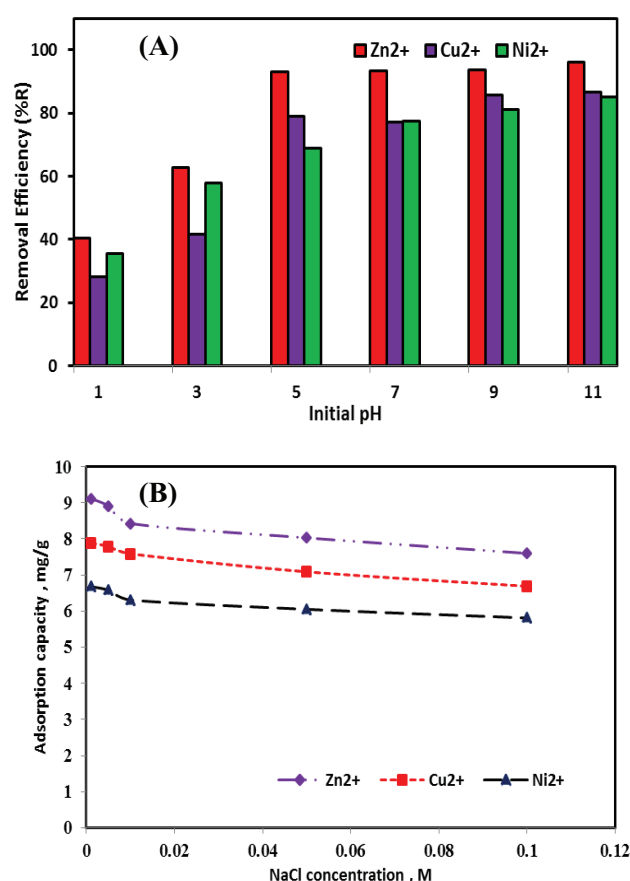
Fig. 4. (A) Effect of pH on adsorption of cations onto the synthesized composite, (B) Effect of ionic strength on the adsorption capacity of Ni^{2+}, Cu^{2+}, Zn^{2+} onto the synthesized composite.

The results revealed that the removal of cations increased from 40.5 to 96.10; 28.10 to 86.60 and 35.5 to 85.60% for Zn^{2+}; Cu^{2+} and Ni^{2+}, respectively. At lower pH value, the surface of the composite was likely to be positively charged thus inhibiting the adsorption of cationic molecules. Conversely, at higher pH value the cations adsorption increase owing to electrostatic interaction [32]. Zinc is the most adsorbed cation due to the fact that the removal percentage is related to the hydrolysis constant of the metallic ion. The degree to which the metals are hydrolyzed is probably the main factor that determines the quantity of metal retained at a given pH [33]. The maximal removal of Zn^{2+}; Cu^{2+} and Ni^{2+} was achieved at pH 11. However, the experiments were carried out at neutral pH value to avert any possible hydroxide precipitation. The inversion in adsorption between Cu^{2+} and Ni^{2+} when pH increases may be explained via the use of visual MINTEQ 6.0 software (Fig. S1). The results of Cu^{2+} speciation depict that free Cu^{2+} ions is the main copper specie till pH 5 then copper hydroxyl species and copper chloride start to buildup. On the other hand, nickel speciation shows that free Ni^{2+} ions are the main specie till pH 8 and nickel chloride species start to appear at pH 5. This means that the inversion at pH 5 occurred due to the increase of the number of appeared species at that pH in case of copper than nickel

as the intensity of adsorption increase as the number of complexes increase.

3.2.2. Effect of ionic strength

The influence of ionic strength on adsorption of Zn^{2+}; Cu^{2+} and Ni^{2+} is shown in Fig. 4B. In this work, the influence of the additional amounts of NaCl was studied at natural pH value. It can be shown that the adsorption capacities decreased with increasing the concentration of NaCl. The increase in the ionic strength value is influenced by the increase in NaCl concentration and more Na^+ ions can screen the adsorbent negative sites, causing the reduce in the electrostatic attractive force, and thus, the adsorbed amount of Zn^{2+}; Cu^{2+} and Ni^{2+} decreases with increasing Na^+ and Cl^- concentration.

3.2.3. Effect of initial metal ion concentration

The metal ions uptake efficiency onto the synthesized material at different initial cation concentrations are illustrated in Fig. 5A. It was shown that Ni^{2+}, Cu^{2+} and Zn^{2+} removal efficiency ($\%R = 100 \times (C_0 - C_e/C_0)$) decreased when their initial concentration increased that ascribed to the decreased availability of active adsorption sites number [32]. At lower initial cations concentration (50 mg/l), the synthesized composite shows to be an acceptable adsorbent for the removal of the concerned cations from the solution with removal efficiency above 70, 79 and 97% for Ni^{2+}, Cu^{2+} and Zn^{2+}, respectively.

3.2.4. The equilibrium adsorption isotherm

Four two-parameter (Langmuir, Freundlich, Temkin and Flory-Huggins) and one three parameter (Toth) isotherm models were elected to correlate the experimental adsorption data of the concerned cations by the synthesized zirconia-magnesia composite to predicted values (Figs. 5B, 5C, 5D, 5E). Adsorption isotherm constants obtained from adsorption isotherm plots with the error function values are listed in Tables 1 and 2. The best-fitted model was preferred on account of the coefficient of determination (R^2 and χ^2 values). Among the five studied models, it was found that the Toth model sufficiently depicts the adsorption data onto the synthesized composite throughout the whole analyzed concentration range due to high R^2 (>0.90 for all adsorbed cations) and the lowest χ^2 values (<1.8 for all the concerned cations), followed by Freundlich; Langmuir and Temkin isotherm models. This perception was expected, since the three-parameter model roughly always fits better than two parameter equations. For Zn^{2+}; Cu^{2+} and Ni^{2+} adsorption onto the synthesized composite, a better regression coefficient was obtained with the Freundlich (rather than the Langmuir) model, which presumes that the adsorption sites are distributed exponentially regarding heat of adsorption. The difference between the R^2 coefficients values for the Freundlich and Langmuir model is extremely small, signifying that the adsorption mechanism is complex and involves a few various sub-mechanisms. Accordingly, the Toth equation, which is a modified form of the Langmuir equation, was elected to represent the equilibrium of Zn^{2+};
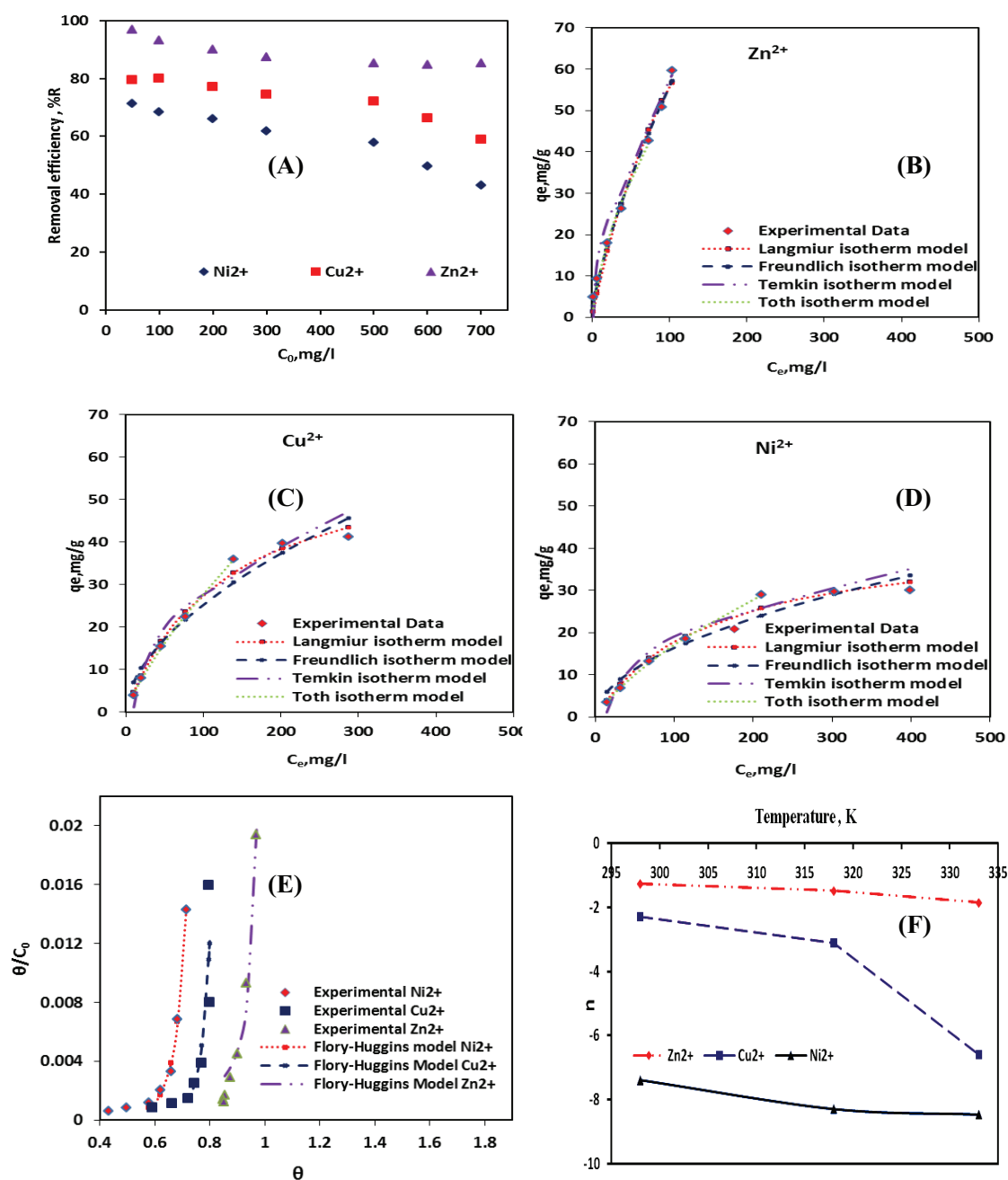
Fig. 5. (A) Ni^{2+}, Cu^{2+}, Zn^{2+} removal efficiency of the synthesized material as a function of different initial ions concentrations (B, C, D, E) Adsorption isotherms of ions onto the material, (F) Variation in the Flory-Huggins adsorption constant *n* with temperature at pH = 7 ± 0.04, adsorbent dose = 10 g/L).

Cu^{2+} and Ni^{2+} adsorption onto zirconia-magnesia composite as follows:

$$q,e,Zn^{2+} = \frac{34.82X0.032C_e}{\left[1 + (0.032C_e)^{0.752}\right]^{\frac{1}{0.752}}} \; ;$$

$$q,e,Ni^{2} = \frac{44.82X0.021C_e}{\left[1 + (0.652C_e)^{0.652}\right]^{\frac{1}{0.652}}}$$

$$q,e,Ni^{2+} = \frac{34.17X0.003C_e}{\left[1 + (0.842C_e)^{0.842}\right]^{\frac{1}{0.842}}}$$

The variance in the amount sorbed of different ions at the same conditions may be owing to the difference in their chemical affinity and adsorption capacity with respect to the chemical functional group on the composite

Table 1
Results of nonlinear isotherm models form Zn^{2+}; Cu^{2+} and Ni^{2+} adsorbed onto the synthesized composite

Ion KK	Langmiur model				Freundlich model				Temkin model					Toth model				
	Q^0 mg/g	b, l/meq	R^2	x^2	K_f mg/g	n	R^2	x^2	b, l/mol	a_t l/g	B_T	R^2	x^2	q_t	K_t	n_t	R^2	x^2
Zn^{2+}	93.74	0.015	0.984	3.22	1.49	1.92	0.992	0.38	266.33	0.76	10.23	0.859	4.33	34.82	0.032	0.752	1.82	
Cu^{2+}	109.09	0.0049	0.993	0.221	1.93	1.79	0.997	0.15	203.22	0.21	13.92	0.911	10.22	44.82	0.021	0.652	0.997	0.041
Ni^{2+}	79.98	0.0042	0.994	0.096	1.49	1.92	0.997	0.09	255.33	0.09	10.22	0.932	3.22	34.72	0.003	0.842	0.018	

Table 2
Flory-Huggins isotherm parameters for Zn^{2+}; Cu^{2+} and Ni^{2+} adsorbed onto the synthesized composite

Temperature, K	Zn^{2+}			Cu^{2+}			Ni^{2+}		
	K_{fh}	n	R^2	K_{fh}	n	R^2	K_{fh}	n	R^2
298	0.00028	1.33	0.981	0.000007	2.91	0.953	0.000004	8.22	0.982
318	0.0001	1.55	0.942	0.000006	2.22	0.962	2.11×10^{-5}	8.02	0.885
333	0.0000007	1.87	0.933	0.000005	5.39	0.942	1.99×10^{-5}	8.82	0.997

surface [27]. To interpret the sorption surface behavior of the concerned cations onto the synthesized composite, the fraction of adsorbent surface covered by the metal cations was also studied via the Flory-Huggins model. The plots of θ/C_0 versus θ were made as shown in Fig. 5E. The Flory-Huggins model was elected to estimate the degree of surface coverage on the composite. The overall coverage process indicates that increase the temperature increases the surface coverage on the composite. Besides, the equilibrium constant, k_{fh} obtained from the Flory-Huggins model was utilized to compute the apparent standard Gibbs free energy of change, ΔG^0, which is the fundamental spontaneity criterion. The negative ΔG^0 values assert the feasibility and spontaneous nature of the adsorption process. Furthermore, the ΔG^0 value became more negative with the increase of temperature, demonstrating that the adsorption process was more favorable at higher temperature [32]. Also, the standard entropy values, ΔS^0 showed increase in the disrandomness or chaos of all the cations adsorption system. The standard enthalpy, ΔH^0 (kJ/mol) value for the removal of zinc and nickel onto the synthesized composite, which was Positive value, thus making this adsorption process endothermic and the ΔH^0 value for the removal of cupper was negative, signifying that this adsorption processes were exothermic (Table 3).

3.2.5. Kinetics modeling

The dynamic experimental data of the concerned cations adsorbed onto the synthesized composite at diverse time intervals and various adsorption temperatures of 298, 318, 333 K was interpreted with fractal like-pseudo-first-; -second-order and Weber–Morris model. The models plots, obtained by nonlinear regression, signify the applicability of both fractal like-pseudo-first- and -second-order models to model the adsorption process kinetics (Fig. 6). It is showed that the adsorption capacity increased with the increase in temperature demonstrating that the sorption process was an endothermic in

Table 3
Thermodynamic parameters values for the adsorption of Zn^{2+}; Cu^{2+} and Ni^{2+} onto the synthesized composite

Cation	Thermodynamic parameter	Temperature, K		
		298	318	333
Zn^{2+}	ΔG^0, kJ/mol	−20.26	−28.38	−35.80
	ΔH^0, kJ/mol	42.87		
	ΔS^0, kJ/K.mol	0.3181		
Cu^{2+}	ΔG^0, kJ/mol	−28.08	−29.08	−30.08
	ΔH^0, kJ/mol	−18.031		
	ΔS^0, kJ/K.mol	0.047		
Ni^{2+}	ΔG^0, kJ/mol	−30.27	−32.16	−33.80
	ΔH^0, kJ/mol	86.72		
	ΔS^0, kJ/K.mol	0.512		

nature and the equilibrium reached within about 40 min. This may be related to the fact that at higher temperature the concerned cations are moving faster, since their hydration radius inversely related with temperature, resulting in higher removal efficiencies. This phenomenon allows ions to diffuse onto the inner part of the pore composite structure. The R^2 values and the error function for adsorption of the cations by the composite are presented in Table 4. It was found that the R^2 and x^2 values, calculated by both models, are close to each other, signifying that the adsorption mechanism onto the composite adsorbent cannot be visibly depicted by one of the two studied models. The fractal like-pseudo-second-order model presumes that the adsorption rate-limiting step is chemisorption amid the cations and the adsorbent binding sites whilst the main fractal like-pseudo-first-order assumption is that the process controlled mostly by physisorption. Thus, the adsorption kinetics of the studied cations onto the synthesized composite cannot be simply determined on the kinetics modelling basis through
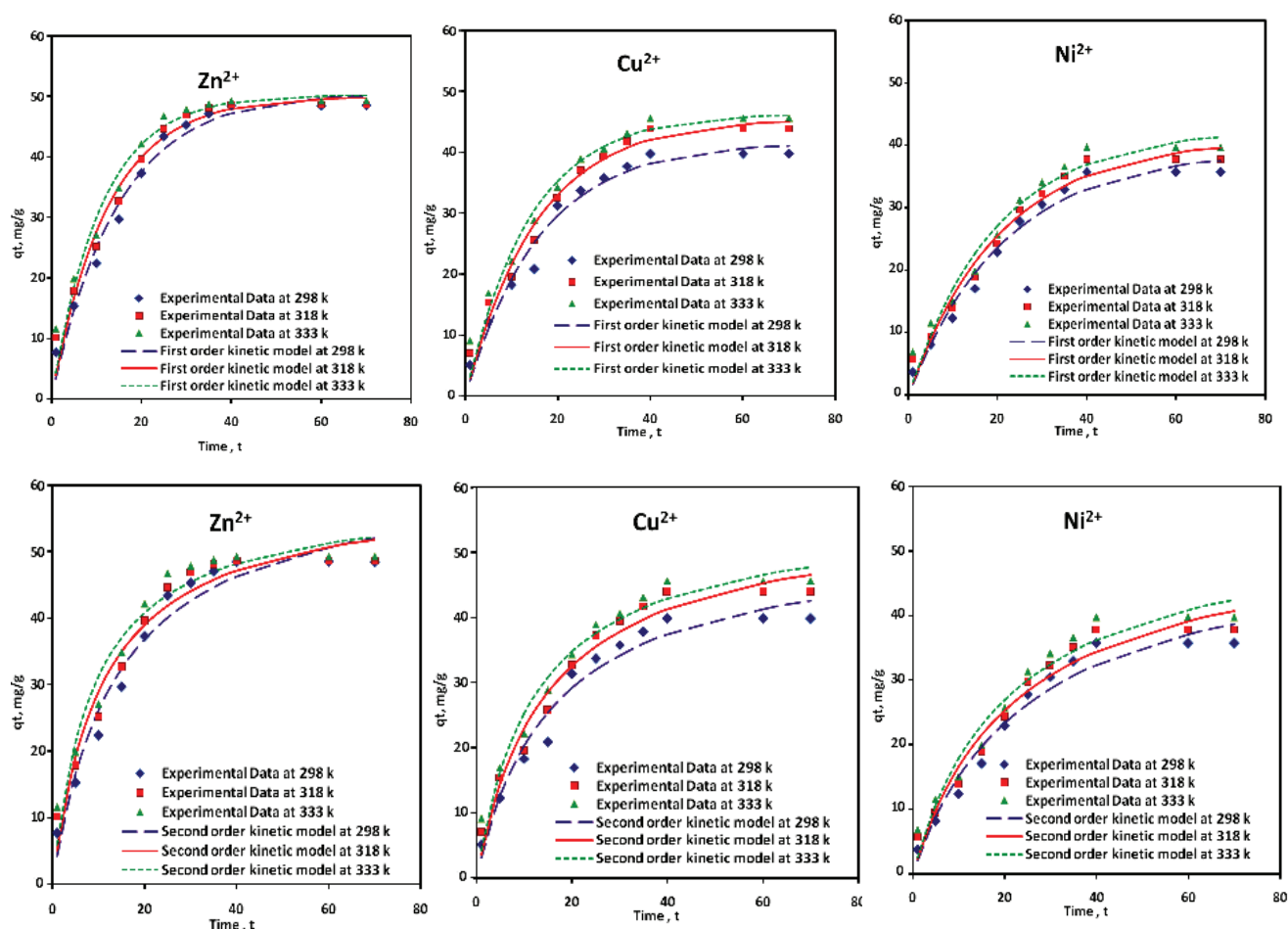
Fig. 6. Pseudo- first- and second-order kinetic model plots for adsorption of zinc, copper and nickel cation at different temperatures, at pH = 7± 0.04, adsorbent dose = 10 g/L.

the reaction adsorption equations. This may propose that adsorption is not a rate-controlling step in the mass transport of cations to the adsorbent surface [26].

The Weber–Morris intra-particle diffusion model plots for Zn^{2+}, Cu^{2+} and Ni^{2+} adsorption onto zirconia-magnesia composite are shown in Fig. 7. The multi-linearity of the intra-particle diffusion plots showed that the cations adsorption onto the composite took place through three stages. The first portion assigned for the diffusion of adsorbate through the solution to the exterior adsorbent surface (from 1 to 15 min). The second portion (from 20 to 35 min) depicts the gradual adsorption stage, where intra-particle diffusion may be the rate limiting step. The third stage (from 40 to 70 min) encompasses the sorbate particles diffusion to adsorption sites. Thus the adsorption mechanism can be considerably controlled by multi-diffusion steps, comprising both film and intra-particle diffusion. The rate constants values are given in Table 4. The obtained intercepts via the extrapolation of the second plot portion back towards the y-axis demonstrated that intra-particle diffusion is not the only process controlling step as the plots do not pass through the origin. It also represents the boundary layer thickness that the tabulated values showed as the intercept

increases as the temperature increase, indicating that more of the adsorbate molecules are being sorbed at the boundary layer. The appeared deviation may be owing to the mass transfer rate differences in the initial and final adsorption stages [34].

3.2.6. Regeneration studies

Rooted in the influence of surface charge on the adsorption process, it was realized that the acid solution can be used to detect desorption of adsorbed Zn^{2+}, Cu^{2+} and Ni^{2+} cations. Two types of acids with various concentrations (0.01–1.0 mol/L), nitric and hydrochloric acids were used to investigate the desorption performance. The desorption efficiency (DE) was estimated using the subsequent equation:

$$DE(\%) = \frac{(C_a - C_d) \cdot 100}{C_a} \tag{16}$$

where C_a and C_d are the concentration of ions adsorbed and desorbed (mg/L), respectively. Three cycles of adsorption-desorption were carried out. It was showed that the

Table 4
Results of the kinetic studies of zinc, copper and nickel cations onto the synthesized composite

Cation	Temp, K	Pseudo-first order				Pseudo-second order				Intra-particle diffusion			
		K_1 min^{-1}	q_{cal} mg/g	R^2	x^2	K_2 g/ mg.min	q_{cal} mg/g	R^2	x^2	time range min	K_2 g/ mg·min	I	R^2
Zn^{2+}	298	0.068	50.5	0.979	0.66	0.072	52. 3	0.963	0.48	1–15	0.735	0	0.993
										20–35	0.658	−0.894	0.960
										40–70	–	–	–
	318	0.081	52.3	0.968	1.11	0.094	58. 5	0.956	0.64	1–15	0.827	0	0.994
										20–35	0.585	−1.431	0.966
										40–70	–	–	–
	333	0.091	55.5	0.959	1.28	0.113	58. 7	0.951	0.68	1–15	0.893	0	0.994
										20–35	0.441	–2.341	0.934
										40–70	–	–	–
Cu^{2+}	298	0.061	41.6	0.975	0.38	0.063	52. 1	0.962	0.31	1–15	0.552	0	0.996
										20–35	0.449	1.122	0.999
										40–70	–	–	–
	318	0.064	45. 5	0.974	0.76	0.068	56. 0	0.966	0.48	1–15	0.655	0	0.995
										20–35	0.618	0.542	0.989
										40–70	–	–	–
	333	0.071	46. 4	0.967	1.17	0.081	56. 1	0.966	0.65	1–15	0.738	0	0.996
										20–35	0.587	0.857	0.984
										40–70	–	–	–
Ni^{2+}	298	0.046	39. 1	0.977	0.32	0.040	52. 3	0.963	0.33	1–15	0.409	0	0.990
										20–35	0.684	0.714	0.990
										40–70	–	–	–
	318	0.048	40. 9	0.972	0.82	0.044	53. 8	0.966	0.68	1–15	0.461	0	0.980
										20–35	0.732	−0.732	0.989
										40–70	–	–	–
	333	0.051	42. 5	0.964	1.23	0.047	55. 1	0.954	0.94	1–15	0.508	0	0.990
										20–35	0.743	−0.683	0.983
										40–70	–	–	–

efficiency of desorption rose with the increase of the acid concentration owing to the enhanced electrostatic repulsion (Fig. 8A). It can be seen from Fig. 8B that the amount of Zn^{2+}, Cu^{2+} and Ni^{2+} desorbed almost remains constant on three cycles. This may be owing to the ignorable amount of composite lost during the cycle experiments. The efficiency of desorption of hydrochloric acid was found to be better than that of nitric acid under the same concentration. Thus, hydrochloric acid (1.0 mol/L) was found to be optimum for desorption of Zn^{2+}, Cu^{2+} and Ni^{2+}, with the DE of 68.7, 83.3 and 96.7%, respectively.

The desorbed composite was activated using (0.01–1.0 mol/L) NaOH solution. Then the regenerated composite was used to adsorb the same concentration of Zn^{2+}, Cu^{2+} and Ni^{2+} to study its removal efficiency. It is showed from Fig. 8C that the %R of the composite is still high, referring that this composite possessed excellent adsorption capacity and the minor decrease in the removal efficiency may

be due to the incomplete desorption of Zn^{2+}, Cu^{2+} and Ni^{2+} adsorbed on the composite.

3.3. Comparative material

Table 5 shows the comparison amid various types of adsorbents, found in literature, and those of the synthesized composite. It can be concluded that the synthesized composite has a high adsorption capacity that can be used for Zn^{2+}, Cu^{2+} and Ni^{2+} trapping from aqueous solutions [35–40].

4. Conclusion

The adsorption of Zn^{2+}, Cu^{2+} and Ni^{2+} onto the synthesized zirconia-magnesia composite was investigated. The adsorption of the concerned cations follows heterogeneous
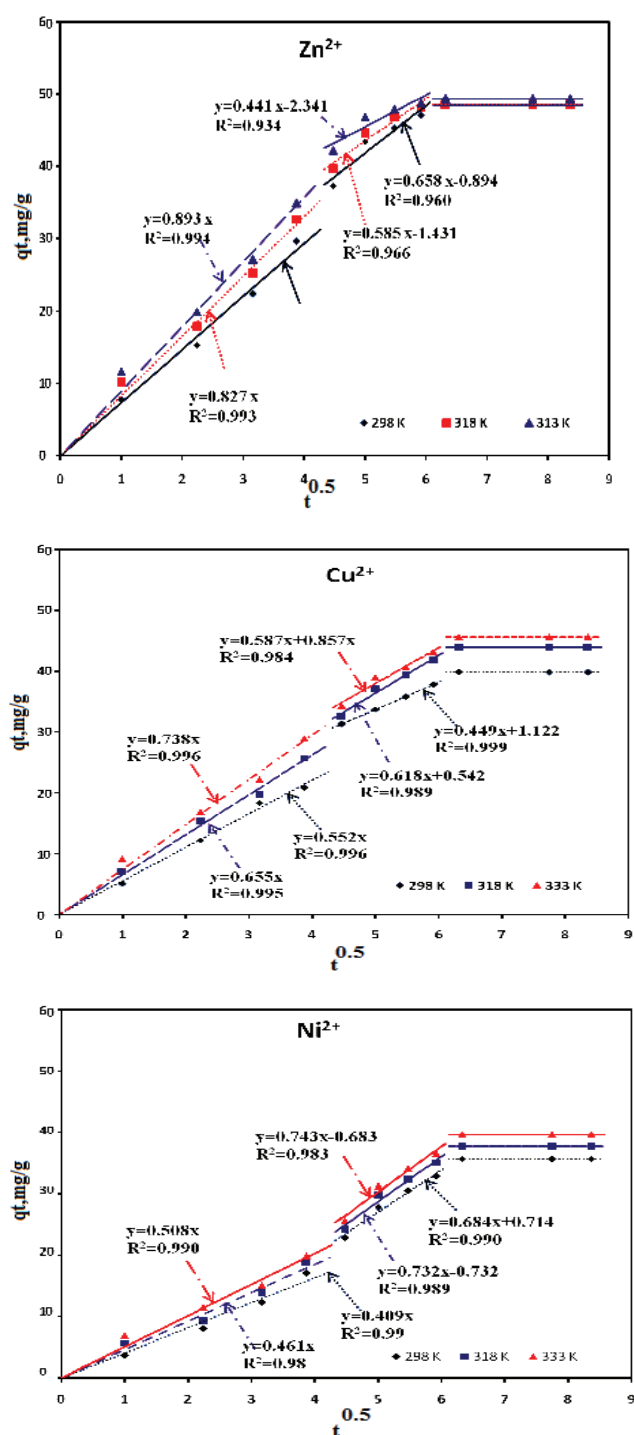
Fig. 7. Adsorption of the concerned cations by the synthesized composite, (A) C_t versus t, (B) early stage plot of q_t versus t and (C) late stage plot of q_t versus t.

Fig. 8. (A) Adsorption performance of the synthesized composite at different acid concentrations, (B) The removal efficiency of zirconia-magnesia composite for Ni^{2+}, Cu^{2+} and Zn^{2+} and (C) Effect of NaOH concentration on the removal efficiency of Ni^{2+}, Cu^{2+} and Zn^{2+}.

surfaces and that the adsorption sites are distributed exponentially regarding heat of adsorption. The Toth model was selected to represent the equilibrium of Zn^{2+}; Cu^{2+} and Ni^{2+} adsorption onto zirconia-magnesia composite. The experimental data were utilized to calculate the ΔG^o values via the use

of Flory-Huggins model, which suggested that adsorption of Zn^{2+}; Cu^{2+} and Ni^{2+} onto zirconia-magnesia composite is spontaneous and an endothermic process. The kinetic study of Zn^{2+}, Cu^{2+} and Ni^{2+} on the synthesized composite was executed rooted in fractal like-pseudo-first-; fractal like-pseudo-second-order and intra-particle diffusion models. It was found that both the fractal like-pseudo-first-; -second-order models are close to each other from R^2 and χ^2 point of view suggesting that the adsorption mechanism onto the adsorbent cannot be obviously depicted by one of the two studied models. The intra-particle diffusion model confirmed that the adsorption mechanism controlled by multi-diffusion steps, comprising both film and intra-particle diffusion.

Desorption studies showed that 1 mol/L hydrochloric acid was a suitable desorpting agent. After activated with 1 mol/L NaOH solution. The synthesized composite could be reused for three times without appreciable loss of its original capacity.

Table 5
Comparison between sorbing materials and the synthesized composite

Sorbing material	Ni^{2+}, mg/g	Zn^{2+}, mg/g	Cu^{2+}, mg/g	References
Natural bentonite	17.20	20.5	28.88	[35]
Chitosan-immobilized on bentonite	6.1	–	12.6	[36]
Sugar cane-based activated carbon	10.03	27.30		[37]
Yellow Loess	1.65	1.65	1.23	[38]
Oil palm and coconut shells-based activated carbons	3.18	–	–	[39]
Wood-activated carbon	–	20.52	–	[40]
Zirconia-magnesia bi-metal composite	79.98	93.74	109.09	Present study

References

[1] J.O. Nrriagu, J.M. Pacyna, Quantitative assessment of world-wide contamination of air, water and soils by trace metals, Nature, 333 (1988) 134–139.

[2] A.K. Bhattacharya, S.N. Mandal, S.K. Das, Adsorption of Zn(II) from aqueous solution by using different adsorbents, Chem. Eng. J., 123 (2006) 43–51.

[3] E. Demirbas, M. Kobya, S. Oncel, S. Sencan, Removal of Ni (II) from aqueous solution by adsorption onto hazelnut shell activated carbon: equilibrium studies, Bioresour. Technol., 84 (2002) 291–293.

[4] D.W. O'Connell, C. Birkinshaw, T.F. O'Dwyer, Heavy metal adsorbents prepared from the modification of cellulose: a review, Bioresour. Technol. 99 (2008) 6709–6724.

[5] M.J. Santos, E. Oliveira, Heavy metals removal in industrial effluents by sequential adsorbent treatment, Adv. Environ. Res., 7 (2003) 263–272.

[6] T. Karthikeyan, S. Rajgopal, L.R. Miranda, Chromium(VI) adsorption from aqueous solution by Hevea Brasilinesis saw-dust activated carbon, J. Hazard. Mater., 124 (2005) 192–199.

[7] L.A. Rodrigues, L.J. Maschio, R.E. da Silva, M.L. da Silva, Adsorption of Cr(VI) from aqueous solution by hydrous zirconium oxide, J. Hazard. Mater., 173 (2010) 630–636.

[8] K. Wu, H. Wang, R. Liu, X. Zhao, H. Liu, J. Qu, Arsenic removal from a high arsenic wastewater using in situ formed Fe–Mn binary oxide combined with coagulation by poly-aluminum chloride, J. Hazard. Mater., 185 (2011) 990–995.

[9] X. Ke , L. Chunguang, L. Juntan, P. Weigong, Study on chromium (VI) removal from aqueous solution using Fe–Mn bimetal oxide, ICETCE, 11 (2011) 1569–1572.

[10] Y. Zhang, M. Yang, M. Dou, H. He, D. Wang, Arsenate adsorption on a Fe–Ce bimetal oxide adsorbent: role of surface properties, Environ. Sci. Technol., 39 (2005) 7246–7253.

[11] Y. Li, B. Gao, T. Wu, D. Sun, X. Li, B. Wang, F. Lu, Hexavalent chromium removal from aqueous solution by adsorption on aluminum magnesium mixed hydroxide, Water Res., 43 (2009) 3067–3075.

[12] B. Chen, Z. Zhu, Y. Guo, Y. Qiu, J. Zhao, Facile synthesis of mesoporous Ce–Fe-bimetal oxide and its enhanced adsorption of arsenate from aqueous solutions, J. Colloid Interface Sci., 398 (2013) 142–151.

[13] Y. Wang, D. Liu, J. Lu, J. Huang, Enhanced adsorption of hexavalent chromium from aqueous solutions on facilely synthesized mesoporous iron–zirconium bimetal oxide, Colloids Surfaces A: Physicochem. Eng. Asp., 481(2015)133–142.

[14] L.J. You, Q. Chen, Y.L. Kang, Y.F. Yu, J.G . He, Evaluation of formation damage using microstructure fractal in shale reservoirs, Fractal, 23 (2015) 154–166.

[15] C.E. Krohn, A.H. Thompson, Fractal sandstone pores: automated measurements using scanning-electron-microscope images, Phys Rev., 33 (1986) 74–83.

[16] A. Malek, S. Farooq, Comparison of isotherm models for hydrocarbon adsorption on activated carbon, AIChE J., 42 (1996) 3191–3201.

[17] I. Langmuir, The constitution and fundamental properties of solids and liquids, J. Am. Chem. Soc., 38 (1916) 2221–2295.

[18] M.M. Dubinin, The potential theory of adsorption of gases and vapors for adsorbents with energetically non-uniform surface, Chem. Rev., 60 (1960) 235–266.

[19] B. Boulinguiez, P. Cloirec, D. Wolbert, Revisiting the determination of Langmuir parameters application to tetrahydrothiophene adsorption onto activated carbon, Langmuir, 24 (2008) 6420–6424.

[20] O.A. Abdel Moamen, H.A. Ibrahim, N. Abdelmonem, I.M. Ismail, Thermodynamic analysis for the sorptive removal of cesium and strontium ions onto synthesized magnetic nano zeolite, Micropor. Mesopor. Mater., 223 (2016) 187–195.

[21] D.A. Ratkowsky, Handbook of Nonlinear Regression Models, Marcel Dekker Inc., New York, 1990.

[22] H.M.F. Freundlich, Über die Adsorption in Lösungen, Z. Phys. Chem-Leipzig, 57 (1906) 385–470.

[23] M.I. Temkin, V. Pyzhev, Kinetics of ammonia synthesis on promoted iron catalyst, Acta Phys. Chim., 12 (1940) 327–356.

[24] J. Toth, State equations of the solid gas interface layer, Acta Chem. Acad. Hung, 69 (1971) 311–317.

[25] Y.S. Ho, J.F. Porter, G. Mckay, Equilibrium isotherm studies for the sorption of divalent metal ions onto peat: copper, nickel and lead single component systems, Water Air Soil Pollut., 141 (2002) 1–33.

[26] M.O. Omorogie, J.O. Babalola, E.I. Unuabonah, J.R., Gong, Clean technology approach for the competitive binding of toxic metal ions onto MnO_2 nanobioextractant, Clean Technol. Environ. Policy., 18 (2016) 171–184.

[27] S. Kundu, A.K. Gupta, Arsenic adsorption onto iron oxide-coated cement (IOCC): regression analysis of equilibrium data with several isotherm models and their optimization, Chem. Eng. J., 122 (2006) 93–106.

[28] O. Palchik, A. Gedanken, Y. Rubinstein, Simple air-tight powder x-ray diffraction cell, Rev. Sci. Instrum., 74 (2003) 3175.

[29] J.L. Murray, The magnesium-aluminum phase diagram, Bull. Alloy Phase Diagrams, 22 (1982) 60–74.

[30] I. Ismail, S.A. Bernal, J.L. Provis, S. Hamdan, J. Deventer, Microstructural changes in alkali activated fly ash/slag geopolymers with sulfate exposure, Mater. Struct., 55 (2013) 361–373.

[31] S. Denkesrenten, Advanced Synthesis of Gold and Zirconia Nanoparticles and their Characterization, deplomica verlag, Hamburg, 2011.

[32] K.T. Jung, A.T. Bell, Synthesis of methanol over zirconia-supported copper, J. Mol. Catal. A: Chem., 163 (2000) 27–42.

[33] R.D. Harter, Effect of soil pH on adsorption of lead, copper, zinc, and nickel, Soil Sci. Soc. Am. J., 47 (1983) 47–51.

[34] R.O. Abdel Rahman, O.A. Abdel Moamen, M. Hanafy, N.M. Abdel Monem, Preliminary investigation of zinc transport through zeolite-X barrier: Linear isotherm assumption, 185 (2012) 61–70.

[35] F. Ghomri, A. Lahsini, A. Laajeb, A. Addaou, The removal of heavy metal ions (copper, zinc, nickel and cobalt) by natural bentonite, Larhyss J., 35 (2013) 37–54.

[36] C. Futalan, T. Sai, S. Lin, M. Dalida, M. Wan, Copper, nickel and lead adsorption from aqueous solution using chitosan-immobilized on bentonite in a ternary system, Sustain. Environ. Res., 22 (2012) 345–355.

[37] F. Taha, F. Kiat, S. Shaharun, A. Ramli, Removal of Ni(II), Zn(II) and Pb(II) cations from single metal aqueous solution using activated carbon prepared from rice husk, Int. J. Env. Chem. Ecolog. Geo. Geophy. Eng., 5 (2011) 112–123.

[38] P. Punrattanasin, P. Sariem, Adsorption of copper, zinc, and nickel using loess as adsorbents, Pol. J. Environ. Stud., 24 (2015) 1259–1266.

[39] L. Gonsalvesh, S.P. Marinov, G. Gryglewicz, R.Carleer, J. Yperman, Preparation, characterization and application of polystyrene based activated carbons for Ni(II) removal from aqueous solution, Fuel Process. Technol., 149 (2016) 75–85.

[40] Rajappa, K. Ramesh, V. Nandhakumar, Adsorption of nickel (II) ion from aqueous solution onto ZnCl$_2$ activated carbon prepared from *Delonix regia* pods (flame tree), IJCPS, 3 (2014) 333–354.

Supplementary file
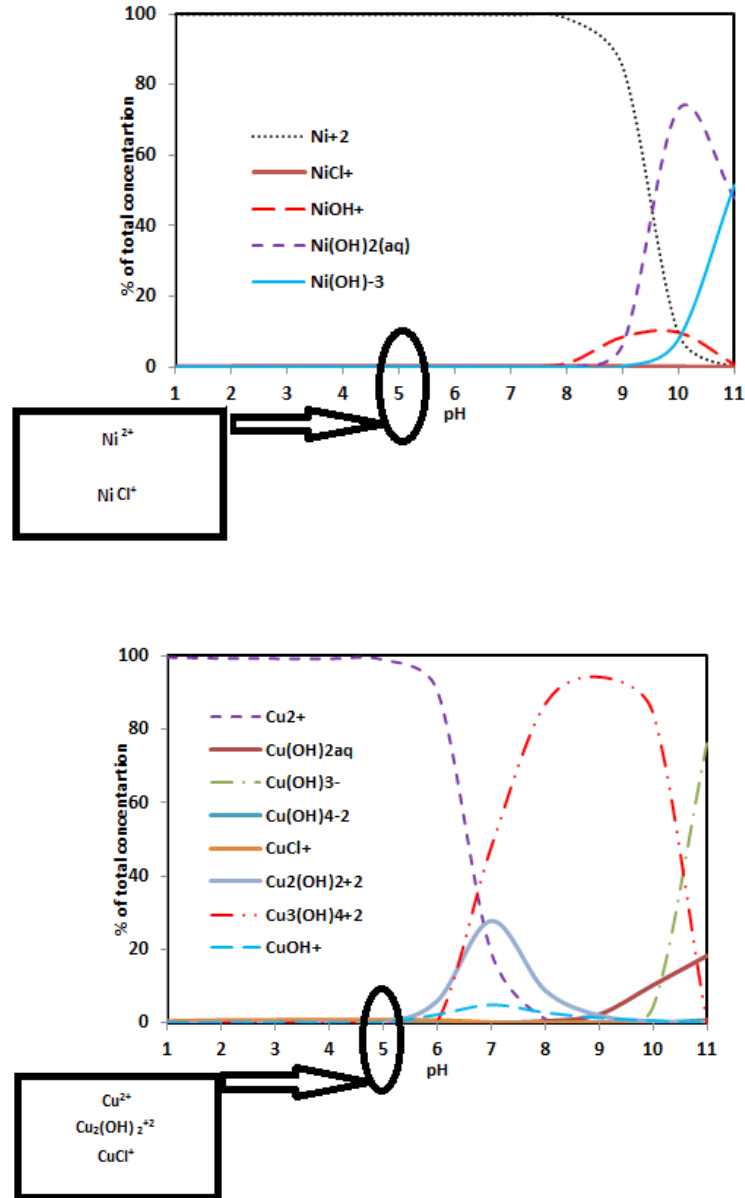
Fig. S1. Distribution of Nickel and copper species as a function of pH.